Nanoscale

COMMUNICATION

View Article Online
View Journal | View Issue

Cite this: *Nanoscale*, 2016, **8**, 7396

Received 12th January 2016,
Accepted 8th March 2016

DOI: 10.1039/c6nr00272b

www.rsc.org/nanoscale

Unraveling a generic growth pattern in structure evolution of thiolate-protected gold nanoclusters†

Wen Wu Xu,[a] Yadong Li,[a,b] Yi Gao*[a,c,d] and Xiao Cheng Zeng*[d,e]

Precise control of the growth of thiolate-protected gold nanoclusters is a prerequisite for their applications in catalysis and bioengineering. Here, we bring to bear a new series of thiolate-protected nanoclusters with a unique growth pattern, *i.e.*, $Au_{20}(SR)_{16}$, $Au_{28}(SR)_{20}$, $Au_{36}(SR)_{24}$, $Au_{44}(SR)_{28}$, and $Au_{52}(SR)_{32}$. These nanoclusters can be viewed as resulting from the stepwise addition of a common structural motif $[Au_8(SR)_4]$. The highly negative values of the nucleus-independent chemical shift (NICS) in the center of the tetrahedral Au_4 units suggest that the overall stabilities of these clusters stem from the local stability of each tetrahedral Au_4 unit. Generalization of this growth-pattern rule to large-sized nanoclusters allows us to identify the structures of three new thiolate-protected nanoclusters, namely, $Au_{60}(SR)_{36}$, $Au_{68}(SR)_{40}$, and $Au_{76}(SR)_{44}$. Remarkably, all three large-sized nanoclusters possess relatively large HOMO–LUMO gaps and negative NICS values, suggesting their high chemical stability. Further extension of the growth-pattern rule to the infinitely long nanowire limit results in a one-dimensional (1D) thiolate-protected gold nanowire (RS-AuNW) with a band gap of 0.78 eV. Such a unique growth-pattern rule offers a guide for precise synthesis of a new class of large-sized thiolate-protected gold nanoclusters or even RS-AuNW which, to our knowledge, has not been reported in the literature.

Introduction

Since the first successful crystallization of the thiolate-protected gold nanocluster $Au_{102}(SR)_{44}$ in 2007,[1] research into the structural evolution and structure–property relationship of thiolate-protected gold nanoclusters has attracted considerable attention due to high potential of these nanoclusters for applications in electronics, catalysis and bioengineering.[2–7] Significant advancement in structure determination has been made on the basis of X-ray crystallography,[1,8–20] single-particle transmission electron microscopy (SP-TEM),[21] as well as density-functional theory (DFT) computation[22–30] in conjunction with the "divide and protect" formulation.[4,31] Although the latter formulation can be very useful in seeking optimal ligand patterns for given gold-core structures, generic growth patterns of the gold nanoclusters are still largely unknown, which hinders the development of large-sized ligand-protected gold nanoclusters for optical and electronic applications.

In this communication, we report a growth-pattern rule that has been revealed based on previously known (*via* X-ray crystallography) and/or theoretically predicted structures of a series of ligand-protected gold nanoclusters, *i.e.*, $Au_{20}(SR)_{16}$,[25,32] $Au_{28}(SR)_{20}$,[13,40] $Au_{36}(SR)_{24}$,[15] $Au_{44}(SR)_{28}$,[28,33] and $Au_{52}(SR)_{32}$.[12] These clusters can be viewed as structural evolutions from the starting cluster $Au_{20}(SR)_{16}$ *via* sequential addition of a $[Au_8(SR)_4]$ motif, *i.e.*, $Au_{20}(SR)_{16} + [Au_8(SR)_4] \rightarrow Au_{28}(SR)_{20} + [Au_8(SR)_4] \rightarrow Au_{36}(SR)_{24} + [Au_8(SR)_4] \rightarrow Au_{44}(SR)_{28} + [Au_8(SR)_4] \rightarrow Au_{52}(SR)_{32}$. Fig. 1 illustrates the structural evolution of the face-centered-cubic (FCC) type of Au kernels in these clusters *via* sequential addition of the "boat-like" Au_8 motif.

Computational methods

All clusters were optimized using the DFT method implemented in the Dmol^3 7.0 code.[34,35] To this end, the generalized gradient approximation in the Perdew–Burke–Ernzerhof (PBE)[36] form was employed together with the double numeric polarized (DNP) basis set and the semi-core pseudopotential. In all our computations, the R group in the ligands is simplified as a methyl group or hydrogen atom. All the optmized structures of the nanoclusters are presented in ESI Fig. S1.† On basis of the optmized structures (R = hydro-

[a]Division of Interfacial Water and Key Laboratory of Interfacial Physics and Technology, Shanghai Institute of Applied Physics, Chinese Academy of Sciences, Shanghai 201800, China. E-mail: gaoyi@sinap.ac.cn
[b]University of Chinese Academy of Sciences, Beijing 100049, China
[c]Shanghai Science Research Center, Chinese Academy of Sciences, Shanghai 201204, China
[d]Department of Chemistry, University of Nebraska-Lincoln, Lincoln, NE 68588, USA. E-mail: xzeng1@unl.edu
[e]Collaborative Innovation Center of Chemistry for Energy Materials, University of Science and Technology of China, Hefei, Anhui 230026, China
†Electronic supplementary information (ESI) available. See DOI: 10.1039/c6nr00272b

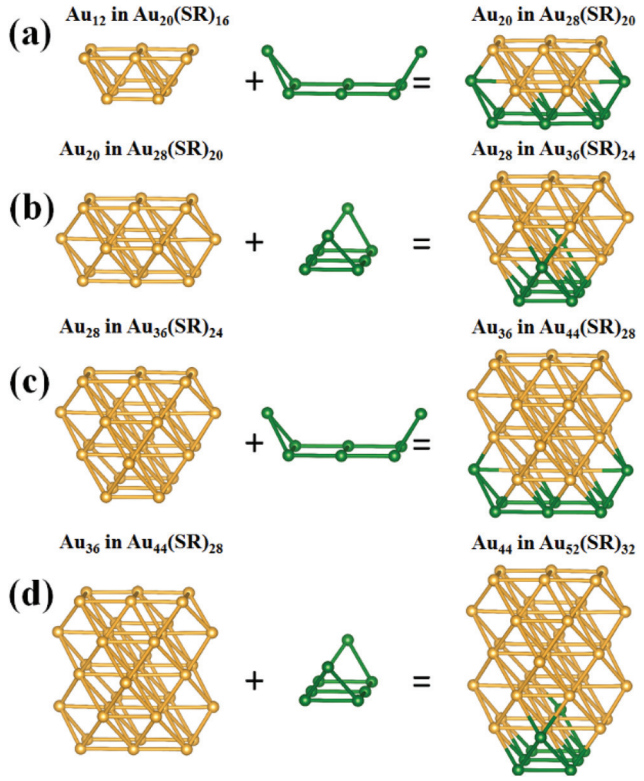

Fig. 1 Au-kernel growth by adding the "boat-like" Au_8 motif (olive). (a) Au_{12} in $Au_{20}(SR)_{16}$ to Au_{20} in $Au_{28}(SR)_{20}$, (b) Au_{20} in $Au_{28}(SR)_{20}$ to Au_{28} in $Au_{36}(SR)_{24}$, (c) Au_{28} in $Au_{36}(SR)_{24}$ to Au_{36} in $Au_{44}(SR)_{28}$, (d) Au_{36} in $Au_{44}(SR)_{28}$ to Au_{44} in $Au_{52}(SR)_{32}$. According to the deduction of Zeng *et al.*,[33] the structures of these nanoclusters can be characterized as $Au_{12}[Au_2(SR)_3]_4(SR)_4$, $Au_{20}[Au_2(SR)_3]_4(SR)_8$/$Au_{20}[Au(SR)_2]_2[Au_2(SR)_3]_2(SR)_8$, $Au_{28}[Au_2(SR)_3]_4(SR)_{12}$, $Au_{36}[Au_2(SR)_3]_4(SR)_{16}$, and $Au_{44}[Au_2(SR)_3]_4(SR)_{20}$, respectively. Next, the Au-kernels can be derived by removing the $[Au_2(SR)_3]$ staple motifs and the bridging thiolates (–SR–).

gen atom), nucleus-independent chemical shift (NICS) analysis was performed to examine the aromaticity of the clusters using the B3LYP functional[37,38] with LANL2DZ and 6-31G* basis set implemented in the Gaussian 09 package.[39]

Results and discussion

As shown in Table 1, the atomic structures of $Au_{28}(SR)_{20}$,[13] $Au_{36}(SR)_{24}$,[15] and $Au_{52}(SR)_{32}$ [20] nanoclusters have been determined *via* X-ray crystallography. Note that $Au_{20}(SR)_{16}$ may have two isomeric structures. The theoretically predicted structure[25] (see Fig. 1(a)) can well reproduce the optical absorption spectrum of $Au_{20}(PET)_{16}$ (PET = SCH_2CH_2Ph),[33] and it has a distinct Au kernel of the crystallized $Au_{20}(TBBT)_{16}$ (TBBT = SPh-*t*-Bu) cluster.[8] However, considering the close total energy of these two structures (their energy difference is 0.3 eV with capped methyl groups for simplicity), one of the two isomers is likely the same as the theoretically predicted structure. A similar situation was reported in the cases of Au_{40}(*o*-MBT)$_{24}$ [43] (*o*-MBT = *ortho*-methylbenzenethiol) and $Au_{40}(PET)_{24}$.[44] The structure prediction of $Au_{44}(SR)_{28}$ [28,33] was based on the structural rules derived from the crystallization of $Au_{28}(SR)_{20}$ and $Au_{36}(SR)_{24}$, *i.e.*, $Au_{28}(SR)_{20}$ + $[Au_8(SR)_4]$ → $Au_{36}(SR)_{24}$ (Fig. 1(b)) + $[Au_8(SR)_4]$ → $Au_{44}(SR)_{28}$ (Fig. 1(c)). The excellent agreement between experimental and computed optical absorption spectra of $Au_{44}(SR)_{28}$ validates the predicted structure of $Au_{44}(SR)_{28}$, which is solely based on the growth-pattern rule derived from $Au_{28}(SR)_{20}$ and $Au_{36}(SR)_{24}$. Additional evidence comes from the crystallization of the $Au_{52}(SR)_{32}$ nanocluster,[20] whose structure can be viewed as adding the $[Au_8(SR)_4]$ motif to the predicted structure of $Au_{44}(SR)_{28}$ (Fig. 1(d)). It should be noted that the recently reported $Au_{28}(S\text{-}c\text{-}C_6H_{11})_{20}$ (where -c-C_6H_{11} = cyclohexyl)[40] cluster exhibits a similar Au_{20} kernel structure to crystallized $Au_{28}(TBBT)_{20}$ (ESI Fig. S2†). Therefore, the two crystallized structures of $Au_{28}(SR)_{20}$ can be evolved from $Au_{20}(SR)_{16}$ (Fig. 1(a)). Besides the different surface-protecting ligands, the two isomeric structures have different staple motifs.

Table 1 A summary of literature results for a series of ligand-protected gold nanoclusters from $Au_{20}(SR)_{16}$ to $Au_{76}(SR)_{44}$. √: structure determined from X-ray crystallography; p: theoretical prediction; \: synthesized clusters without crystallization; ?: structure unknown; ‡: difference in crystallization, prediction not yet confirmed

	Experiment	Theory
$Au_{20}(SR)_{16}$	‡ (ref. 8 and 32)	p (ref. 25)
$Au_{28}(SR)_{20}$	√ (ref. 13 and 40)	√ (ref. 41)
$Au_{36}(SR)_{24}$	√ (ref. 15)	√ (ref. 9)
$Au_{44}(SR)_{28}$	\ (ref. 33)	p (ref. 28 and 42)
$Au_{52}(SR)_{32}$	√ (ref. 20)	?
$Au_{60}(SR)_{36}$	?	This work
$Au_{68}(SR)_{40}$	?	This work
$Au_{76}(SR)_{44}$	\ (ref. 43)	This work

According to the "divide and protect" formulation,[45] $Au_{20}(SR)_{16}$, $Au_{28}(SR)_{20}$, $Au_{36}(SR)_{24}$, $Au_{44}(SR)_{28}$, and $Au_{52}(SR)_{32}$ can be divided into $Au_8[Au_3(SR)_4]_4$, $Au_{14}[Au_2(SR)_3]_4[Au_3(SR)_4]_2$/$Au_{14}[Au(SR)_2]_2[Au_2(SR)_3]_4$, $Au_{20}[Au_2(SR)_3]_8$, $Au_{26}[Au(SR)_2]_2$-$[Au_2(SR)_3]_8$, and $Au_{32}[Au(SR)_2]_4[Au_2(SR)_3]_8$, respectively. The Au_8 in $Au_{20}(SR)_{16}$, Au_{14} in $Au_{28}(SR)_{20}$, Au_{20} in $Au_{36}(SR)_{24}$, Au_{26} in $Au_{44}(SR)_{28}$, and Au_{32} in $Au_{52}(SR)_{32}$, which are comprised of tetrahedral Au_4 units, can be derived by removing the $[Au(SR)_2]$, $[Au_2(SR)_3]$, and $[Au_3(SR)_4]$ staple motifs, as shown in Fig. 2. It is known that NICS values have been commonly used as an index to measure the local aromaticity of fullerene cages[46] or small metal clusters.[47] In addition, NICS analyses have been applied successfully to evaluate the stabilities of gold fullerene structures, such as Au_{32} [48] and Au_{42}.[49] Recently, NICS analyses of the $Au_{20}(SR)_{16}$ cluster were performed to support the concept of a superatom-network (SAN);[50] a theory to explain the stability of thiolate-protected gold nanoclusters. Thus, it is sensible to examine the stabilities of $Au_{20}(SR)_{16}$, $Au_{28}(SR)_{20}$, $Au_{36}(SR)_{24}$, $Au_{44}(SR)_{28}$, and $Au_{52}(SR)_{32}$ based on the computed NICS values corresponding to the center of the tetrahedral Au_4 units of these clusters. It can be seen that the absolute NICS values (see Table 2) at the centers of the tetra-

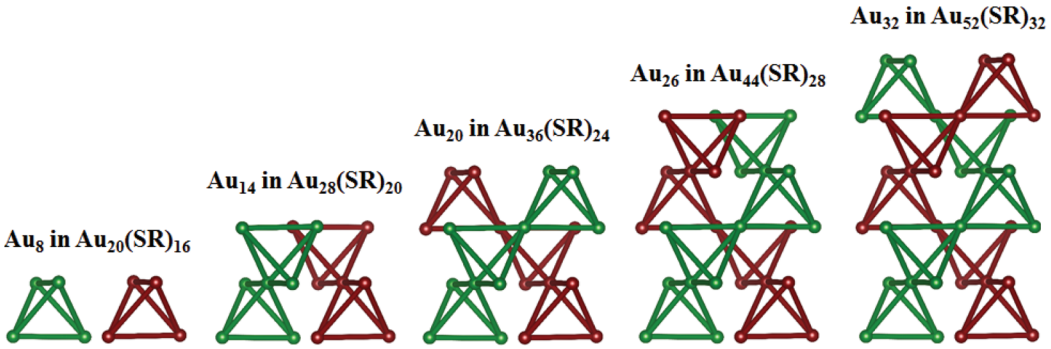

Fig. 2 The structures of Au_8 in $Au_{20}(SR)_{16}$, Au_{14} in $Au_{28}(SR)_{20}$, Au_{20} in $Au_{36}(SR)_{24}$, Au_{26} in $Au_{44}(SR)_{28}$, and Au_{32} in $Au_{52}(SR)_{32}$. Au atoms are both olive and wine.

Table 2 Computed nucleus-independent chemical shift (NICS) values of $Au_{20}(SR)_{16}$, $Au_{28}(SR)_{20}$, $Au_{36}(SR)_{24}$, $Au_{44}(SR)_{28}$, and $Au_{52}(SR)_{32}$. "0" denotes the NICS values at the centers of the total structures. "1–10" denote the NICS values at the centers of tetrahedral Au_4 units of these clusters (ESI Fig. S3)

	0	1	2	3	4	5	6	7	8	9	10
$Au_{20}(SR)_{16}$	−7.5	−28.2	−28.7								
$Au_{28}(SR)_{20}$	−12.4	−25.3	−26.3	−25.2	−26.5						
$Au_{36}(SR)_{24}$	−10.8	−24.5	−26.2	−23.4	−25.1	−24.2	−25.7				
$Au_{44}(SR)_{28}$	−17.3	−25.6	−23.5	−23.5	−25.6	−25.6	−23.8	−23.5	−25.6		
$Au_{52}(SR)_{32}$	−12.7	−25.9	−25.1	−24.2	−22.1	−25.5	−26.0	−23.1	−23.0	−24.7	−25.7

hedral Au_4 units are large; larger than those at the centers of the total structures. The NICS results suggest notable aromaticity in the tetrahedral Au_4 units. As such, the overall stabilities of $Au_{20}(SR)_{16}$, $Au_{28}(SR)_{20}$, $Au_{36}(SR)_{24}$, $Au_{44}(SR)_{28}$, and $Au_{52}(SR)_{32}$ likely stem from the local stability of each tetrahedral Au_4 unit.

The unique growth-pattern rule derived among the series of clusters, $Au_{20}(SR)_{16}$, $Au_{28}(SR)_{20}$, $Au_{36}(SR)_{24}$, $Au_{44}(SR)_{28}$ and $Au_{52}(SR)_{32}$, suggests the possible existence of larger-sized clusters through continuously adding the motif $[Au_8(SR)_4]$, *e.g.*, $Au_{52}(SR)_{32} + [Au_8(SR)_4] \rightarrow Au_{60}(SR)_{36} + [Au_8(SR)_4] \rightarrow Au_{68}(SR)_{40} + [Au_8(SR)_4] \rightarrow Au_{76}(SR)_{44}$, where the newly created $Au_{60}(SR)_{36}$, $Au_{68}(SR)_{40}$, and $Au_{76}(SR)_{44}$ all possess the FCC-type Au-kernels (Fig. 3). Fig. 4 presents the computed HOMO–LUMO gaps of the optimized nanoclusters from the small-sized $Au_{20}(SR)_{16}$ to large-sized $Au_{76}(SR)_{44}$, as well as the experimentally measured optical gaps of $Au_{20}(SR)_{16}$, $Au_{28}(SR)_{20}$, $Au_{36}(SR)_{24}$, and $Au_{44}(SR)_{28}$. The computed gaps reproduce the experimental gaps quite well except for $Au_{28}(SR)_{20}$. Nevertheless, the computed gap of $Au_{28}(SR)_{20}$ is consistent with a previous theoretical study.[14] The HOMO–LUMO gaps of $Au_{60}(SR)_{36}$, $Au_{68}(SR)_{40}$, and $Au_{76}(SR)_{44}$ are all greater than 1.0 eV, comparable to those of $Au_{64}(SC_6H_{11})_{32}$ [51] and $Au_{67}(PET)_{35}$.[52] Double-helix structures made of tetrahedral Au_4 units can be seen in the three new structures (ESI Fig. S4†), and are also present in $Au_{20}(SR)_{16}$, $Au_{28}(SR)_{20}$, $Au_{36}(SR)_{24}$, $Au_{44}(SR)_{28}$ and $Au_{52}(SR)_{32}$ clusters. Furthermore, the NICS analyses (ESI Table S1 and Fig. S6†) also show that the overall stabilities of $Au_{60}(SR)_{36}$, $Au_{68}(SR)_{40}$, and $Au_{76}(SR)_{44}$ are likely due to the local stability

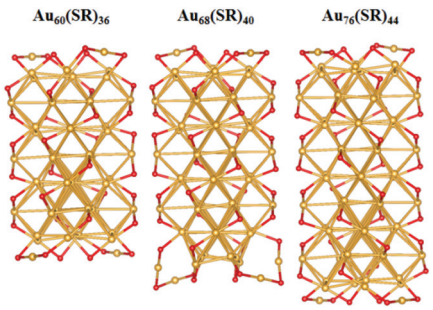

Fig. 3 The optimized structures of $Au_{60}(SR)_{36}$, $Au_{68}(SR)_{40}$, and $Au_{76}(SR)_{44}$, where the methyl groups are omitted for clarity. Au and S atoms are in gold and red, respectively.

of each tetrahedral Au_4 unit. The large HOMO–LUMO gaps and the negative NICS values suggest high stability of the newly predicted structures.

It should be noted that the Au_{76}(4-MEBA)$_{44}$ (4-MEBA = 4-(2-mercaptoethyl)benzoic acid) nanocluster has been synthesized recently by Takano *et al.*[53] Although Au_{76}(4-MEBA)$_{44}$ has the same number of Au atoms and ligands as $Au_{76}(SR)_{44}$, a comparison of the computed and experimental X-ray diffraction (XRD) and optical absorption spectra suggests that the two clusters may have different structures in their Au-kernels (ESI Fig. S5†). It is known that surface-protecting thiolates can have significant effects on the structures of gold nanoclusters even with the same number of Au and S atoms. For example, the marked differences in their absorption spectra indicate that

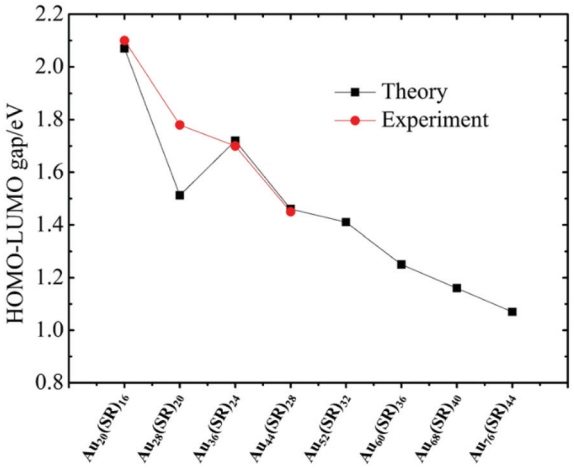

Fig. 4 The computed HOMO–LUMO gaps of the optimized nanoclusters from small-sized $Au_{20}(SR)_{16}$ to large-sized $Au_{76}(SR)_{44}$, and the measured optical gaps.

$Au_{40}(o\text{-MBT})_{24}$ [43] and $Au_{40}(PET)_{24}$ [44] have different structures, and so do $Au_{20}(PET)_{16}$ [32] and $Au_{20}(TBBT)_{16}$,[8] as well as $Au_{28}(TBBT)_{20}$ [13] and $Au_{28}(S\text{-}c\text{-}C_6H_{11})_{20}$.[40] Moreover, even with the same ligands, different $Au_{38}(PET)_{24}$ isomers have been detected.[15,54]

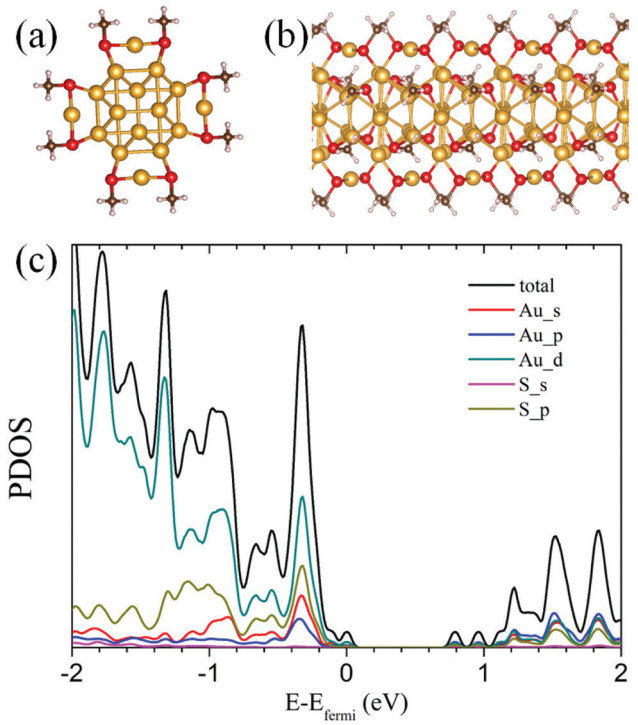

Fig. 5 The proposed structure of the thiolate-protected gold nanowire: (a) viewed along the wire; (b) side view. Au, S, C, and H atoms are in gold, red, dark gray, and white, respectively. (c) Computed projected density of state (PDOS) of the thiolate-protected gold nanowire. Au_s, Au_p, and Au_d denote the s, p, and d orbitals of Au atoms, respectively. S_s and S_p denote the s and p orbitals of S atoms, respectively.

Lastly, if the growth-pattern rule is extended to the infinitely-long nanowire limit by repeatedly adding $[Au_8(SR)_4]$ units in one direction, the thiolate-protected gold nanowire (RS-AuNW) can be obtained, as shown in Fig. 5(a) and (b). The present RS-AuNW also exhibits a double-helix structure made of tetrahedral Au_4 units, which is very different from that of previously proposed vertex- and face-sharing icosahedral thiolated Au nanowires[55] and crystallized $[Au_{25}(SBu)_{18}^0]_n$ nanowires.[56] Fig. 5(c) shows the computed total density of state (DOS) of the present RS-AuNW, which shows an electronic band gap of 0.78 eV, suggesting that the present RS-AuNW is semiconducting. The vertex-sharing thiolated gold nanowire can be made either semiconducting or metallic by tuning the charge. The face-sharing nanowire is always metallic. The non-magnetic ground state of $[Au_{25}(SBu)_{18}^0]_n$ has a band gap of 0.12 eV, suggesting that $[Au_{25}(SBu)_{18}^0]_n$ could behave as a narrow-gap semiconductor. It is also found that the valence band of the present RS-AuNW is mainly contributed to by the Au(5d), S(3p) Au(6s), and Au(6p) atomic orbitals, while the conduction band is mainly due to the Au(6sp) atomic orbitals.

Conclusions

In conclusion, a generic growth-pattern rule is identified based on the series of nanoclusters $Au_{20}(SR)_{16}$, $Au_{28}(SR)_{20}$, $Au_{36}(SR)_{24}$, $Au_{44}(SR)_{28}$, and $Au_{52}(SR)_{32}$, which can be viewed as the sequential addition of $[Au_8(SR)_4]$ units. The large negative nucleus-independent chemical shift (NICS) values in the centers of the tetrahedral Au_4 units indicate that the integral stabilities of these clusters are determined by the local stability of each tetrahedral Au_4 unit. Extension of the rule to larger-sized nanoclusters than the state-of-the-art gives rise to new structures of nanoclusters such as $Au_{60}(SR)_{36}$, $Au_{68}(SR)_{40}$, and $Au_{76}(SR)_{44}$. All three large-sized nanoclusters exhibit relatively large HOMO–LUMO gaps and negative NICS values, suggesting their high chemical stability. It is also found that the computed XRD and optical absorption spectra of $Au_{76}(SR)_{44}$ are not the same as those of $Au_{76}(4\text{-MEBA})_{44}$ from experiments, suggesting the two nanoclusters may have different Au-kernel structures. Finally, extension of the growth-pattern rule to the infinitely long nanowire limit results in a 1D RS-AuNW with a band gap of 0.78 eV. The unique growth-pattern rule offers a guide for future synthesis of a new class of large-sized thiolate-protected gold nanoclusters or even RS-AuNW that has not been reported in the literature.

Acknowledgements

W.W.X. is supported by the China postdoctoral science foundation project (Y419022011, Y519031011), and National Natural Science Foundation of China (11504396). Y.G. is supported by start-up funding from the Shanghai Institute of Applied Physics, Chinese Academy of Sciences (Y290011011), National Natural Science Foundation of China (21273268,

11574340), "Hundred People Project" from Chinese Academy of Sciences, "Pu-jiang Rencai Project" from Science and Technology Commission of Shanghai Municipality (13PJ1410400), and CAS-Shanghai Science Research Center (CAS-SSRC-YJ-2015-01). The computational resources utilized in this research were provided by Shanghai Supercomputer Center, National Supercomputer Centers in Tianjin and Shenzhen, and special program for applied research on super-computation of the NSFC-Guangdong joint fund (the second phase). X.C.Z. is supported by the USTC Qian-ren B (1000-Talents Program B) fund for summer research.

References

1 P. D. Jadzinsky, G. Calero, C. J. Ackerson, D. A. Bushnell and R. D. Kornberg, *Science*, 2007, **318**, 430–433.
2 R. Jin, *Nanoscale*, 2010, **2**, 343–362.
3 H. Häkkinen, *Nat. Chem.*, 2012, **4**, 443–455.
4 Y. Pei and X. C. Zeng, *Nanoscale*, 2012, **4**, 4054–4072.
5 H. Qian, M. Zhu, Z. Wu and R. Jin, *Acc. Chem. Res.*, 2012, **45**, 1470–1479.
6 R. Jin, *Nanoscale*, 2015, **7**, 1549–1565.
7 R. W. Murray, *Chem. Rev.*, 2008, **108**, 2688–2720.
8 A. Das, C. Liu, H. Y. Byun, K. Nobusada, S. Zhao, N. Rosi and R. Jin, *Angew. Chem., Int. Ed.*, 2015, **54**, 3140–3144.
9 C. Zeng, C. Liu, Y. Chen, N. L. Rosi and R. Jin, *J. Am. Chem. Soc.*, 2014, **136**, 11922–11925.
10 D. Crasto, G. Barcaro, M. Stener, L. Sementa, A. Fortunelli and A. Dass, *J. Am. Chem. Soc.*, 2014, **136**, 14933–14940.
11 M. Zhu, C. M. Aikens, F. J. Hollander, G. C. Schatz and R. Jin, *J. Am. Chem. Soc.*, 2008, **130**, 5883–5885.
12 M. W. Heaven, A. Dass, P. S. White, K. M. Holt and R. W. Murray, *J. Am. Chem. Soc.*, 2008, **130**, 3754–3755.
13 C. Zeng, T. Li, A. Das, N. L. Rosi and R. Jin, *J. Am. Chem. Soc.*, 2013, **135**, 10011–10013.
14 D. Crasto, S. Malola, G. Brosofsky, A. Dass and H. Häkkinen, *J. Am. Chem. Soc.*, 2014, **136**, 5000–5005.
15 C. Zeng, H. Qian, T. Li, G. Li, N. L. Rosi, B. Yoon, R. N. Barnett, R. L. Whetten, U. Landman and R. Jin, *Angew. Chem., Int. Ed.*, 2012, **51**, 13114–13118.
16 H. Qian, W. T. Eckenhoff, Y. Zhu, T. Pintauer and R. Jin, *J. Am. Chem. Soc.*, 2010, **132**, 8280–8281.
17 Y. Chen, C. Zeng, C. Liu, K. Kirschbaum, C. Gayathri, R. R. Gil, N. L. Rosi and R. Jin, *J. Am. Chem. Soc.*, 2015, **137**, 10076–10079.
18 A. Dass, S. Theivendran, P. R. Nimmala, C. Kumara, V. R. Jupally, A. Fortunelli, L. Sementa, G. Barcaro, X. Zuo and B. C. Noll, *J. Am. Chem. Soc.*, 2015, **137**, 4610–4613.
19 C. Zeng, Y. Chen, K. Kirschbaum, K. Appavoo, M. Y. Sfeir and R. Jin, *Sci. Adv.*, 2015, **1**, e1500045.
20 C. Zeng, Y. Chen, C. Liu, K. Nobusada, N. L. Rosi and R. Jin, *Sci. Adv.*, 2015, **1**, e1500425.
21 M. Azubel, J. Koivisto, S. Malola, D. Bushnell, G. L. Hura, A. L. Koh, H. Tsunoyama, T. Tsukuda, M. Pettersson, H. Häkkinen and R. D. Kornberg, *Science*, 2014, **345**, 909–912.
22 J. Akola, M. Walter, R. L. Whetten, H. Häkkinen and H. Grönbeck, *J. Am. Chem. Soc.*, 2008, **130**, 3756–3757.
23 W. W. Xu, Y. Gao and X. C. Zeng, *Sci. Adv.*, 2015, **1**, e1400211.
24 W. W. Xu and Y. Gao, *J. Phys. Chem. C*, 2015, **119**, 14224–14229.
25 Y. Pei, Y. Gao, N. Shao and X. C. Zeng, *J. Am. Chem. Soc.*, 2009, **131**, 13619–13621.
26 Y. Pei, R. Pal, C. Liu, Y. Gao, Z. Zhang and X. C. Zeng, *J. Am. Chem. Soc.*, 2012, **134**, 3015–3024.
27 Y. Pei, Y. Gao and X. C. Zeng, *J. Am. Chem. Soc.*, 2008, **130**, 7830–7832.
28 Y. Pei, S. S. Lin, J. Su and C. Liu, *J. Am. Chem. Soc.*, 2013, **135**, 19060–19063.
29 Y. Pei, J. Tang, X. Tang, Y. Huang and X. C. Zeng, *J. Phys. Chem. Lett.*, 2015, **6**, 1390–1395.
30 D. Jiang, S. H. Overbury and S. Dai, *J. Am. Chem. Soc.*, 2013, **135**, 8786–8789.
31 H. Häkkinen, M. Walter and H. Gronbeck, *J. Phys. Chem. B*, 2006, **110**, 9927–9931.
32 M. Zhu, H. Qian and R. Jin, *J. Am. Chem. Soc.*, 2009, **131**, 7220–7221.
33 C. Zeng, Y. Chen, G. Li and R. Jin, *Chem. Commun.*, 2014, **50**, 55–57.
34 B. Delley, *J. Chem. Phys.*, 1990, **92**, 508–517.
35 B. Delley, *J. Chem. Phys.*, 2003, **113**, 7756–7764. Dmol^3 is available from Accelrys.
36 J. P. Perdew, K. Burke and M. Ernzerhof, *Phys. Rev. Lett.*, 1996, **77**, 3865–3868.
37 A. D. Becke, *Phys. Rev. A*, 1988, **38**, 3098.
38 A. Lee, W. Yang and R. G. Parr, *Phys. Rev. B: Condens. Matter*, 1988, **37**, 785–789.
39 M. J. Frisch, G. W. Trucks, H. B. Schlegel, G. E. Scuseria, M. A. Robb, J. R. Cheeseman, V. G. Zakrzewski, J. A. Montgomery Jr., R. E. Stratmann, J. C. Burant, S. Dapprich, J. M. Millam, A. D. Daniels, K. N. Kudin, M. C. Strain, O. Farkas, J. Tomasi, V. Barone, M. Cossi, R. Cammi, B. Mennucci, C. Pomelli, C. Adamo, S. Clifford, J. Ochterski, G. A. Petersson, P. Y. Ayala, Q. Cui, K. Morokuma, D. K. Malick, A. D. Rabuck, K. Raghavachari, J. B. Foresman, J. Cioslowski, J. V. Ortiz, B. B. Stefanov, G. Liu, A. Liashenko, P. Piskorz, I. Komaromi, R. Gomperts, R. L. Martin, D. J. Fox, T. Keith, M. A. Al-Laham, C. Y. Peng, A. Nanayakkara, C. Gonzalez, M. Challacombe, P. M. W. Gill, B. Johnson, W. Chen, M. W. Wong, J. L. Andres, C. Gonzalez, M. Head-Gordon, E. S. Replogle and J. A. Pople, *Gaussian09 (Revision A.02)*, Gaussian, Inc., Wallingford CT, 2009.
40 Y. Chen, C. Liu, Q. Tang, C. Zeng, T. Higaki, A. Das, D. Jiang, N. L. Rosi and R. Jin, *J. Am. Chem. Soc.*, 2016, **138**, 1482–1485.
41 S. K. Knoppe, S. Malola, T. Burgi and H. Häkkinen, *J. Phys. Chem. A*, 2013, **117**, 10526–10533.

42 D. Jiang, M. Walter and J. Akola, *J. Phys. Chem. C*, 2010, **114**, 15883–15889.
43 Y. Chen, C. Zeng, D. R. Kauffman and R. Jin, *Nano Lett.*, 2015, **15**, 3603–3609.
44 H. Qian, Y. Zhu and R. Jin, *J. Am. Chem. Soc.*, 2010, **132**, 4583–4585.
45 H. Häkkinen, M. Walter and H. Gronbeck, *J. Phys. Chem. B*, 2006, **110**, 9927–9931.
46 A. Hirsch, Z. Chen and H. Jiao, *Angew. Chem., Int. Ed.*, 2000, **39**, 3915–3917.
47 I. Boldyrev and L. S. Wang, *Chem. Rev.*, 2005, **105**, 3716–3757.
48 M. P. Johansson, D. Sundholm and J. Vaara, *Angew. Chem., Int. Ed.*, 2004, **43**, 2678–2681.
49 Y. Gao and X. C. Zeng, *J. Am. Chem. Soc.*, 2005, **127**, 3698–3699.
50 L. Cheng, Y. Yuan, X. Zhang and J. Yang, *Angew. Chem., Int. Ed.*, 2013, **52**, 9035–9039.
51 C. Zeng, Y. Chen, G. Li and R. Jin, *Chem. Mater.*, 2014, **26**, 2635–2641.
52 P. R. Nimmala, B. Yoon, R. L. Whetten, U. Landman and A. Dass, *J. Phys. Chem. A*, 2013, **117**, 504–517.
53 S. Takano, S. Yamazoe, K. Koyasu and T. Tsukuda, *J. Am. Chem. Soc.*, 2015, **137**, 7027–7030.
54 S. Tian, Y. Li, M. Li, J. Yuan, J. Yang, Z. Wu and R. Jin, *Nat. Commun.*, 2015, **6**, 8667.
55 D. Jiang, K. Nobusada, W. Luo and R. L. Whetten, *ACS Nano*, 2009, **3**, 2351–2357.
56 M. D. Nardi, S. Antonello, D. Jiang, F. Pan, K. Rissanen, M. Ruzzi, A. Venzo, A. Zoleo and F. Maran, *ACS Nano*, 2014, **8**, 8505–8512.